

# Antireflection effects at nanostructured material interfaces and the suppression of thin-film interference

Qiaoyin Yang<sup>1</sup>, Xu A Zhang<sup>1</sup>, Abhijeet Bagal<sup>1</sup>, Wei Guo<sup>2</sup> and Chih-Hao Chang<sup>1</sup>

<sup>1</sup> Department of Mechanical and Aerospace Engineering, North Carolina State University, Raleigh, NC 27695, USA

<sup>2</sup> Department of Materials Science and Engineering, North Carolina State University, Raleigh, NC 27695, USA

E-mail: [chichang@ncsu.edu](mailto:chichang@ncsu.edu)


Received 12 February 2013, in final form 4 April 2013

Published 15 May 2013

Online at [stacks.iop.org/Nano/24/235202](http://stacks.iop.org/Nano/24/235202)

## Abstract

Thin-film interference is a well-known effect, and it is commonly observed in the colored appearance of many natural phenomena. Caused by the interference of light reflected from the interfaces of thin material layers, such interference effects can lead to wavelength and angle-selective behavior in thin-film devices. In this work, we describe the use of interfacial nanostructures to eliminate interference effects in thin films. Using the same principle inspired by moth-eye structures, this approach creates an effective medium where the index is gradually varying between the neighboring materials. We present the fabrication process for such nanostructures at a polymer–silicon interface, and experimentally demonstrate its effectiveness in suppressing thin-film interference. The principle demonstrated in this work can lead to enhanced efficiency and reduce wavelength/angle sensitivity in multilayer optoelectronic devices.

 Online supplementary data available from [stacks.iop.org/Nano/24/235202/mmedia](http://stacks.iop.org/Nano/24/235202/mmedia)

(Some figures may appear in colour only in the online journal)

## 1. Introduction

In recent years, there has been significant research interest in antireflection (AR) nanostructures that suppress Fresnel reflection from material surfaces [1–21]. Inspired by the moth eye, the subwavelength structures create an effective medium with a gradient-index profile for optical impedance matching [1–5]. Such a bio-inspired nanostructured surface has demonstrated antireflection effects over broadband and wide-angle illumination, which is advantageous over traditional AR coating. Engineered surfaces using techniques such as electron-beam lithography [6, 7], interference lithography [8–10], colloidal self-assembly [11–14], self-masking etching [15] and polymer replication [16–19] have been implemented to effectively suppress surface reflections. Oblique-angle deposition of multilayers with varying porosity

is also effective in emulating a gradient-index medium [20, 21]. These advances have significant applications in improving the efficiency of solar cells [9, 21–28], enhancing light extraction in light emitting devices [29] and enabling anti-glare, self-cleaning windows for displays [10].

In addition to surface reflection, refractive-index mismatch can also cause reflections at the interface between two materials. These reflections can lead to significant transmission losses in devices with multilayer stacks. In addition, multiple reflections in thin films also cause optical interference when the film thickness is within the coherence length of the incident light source. This effect, as depicted in figure 1, results in wavelength- and angle-dependent transmittance and reflectance, leading to the colored appearance commonly observed in thin-film devices. While thin-film interference effects can be designed to be useful

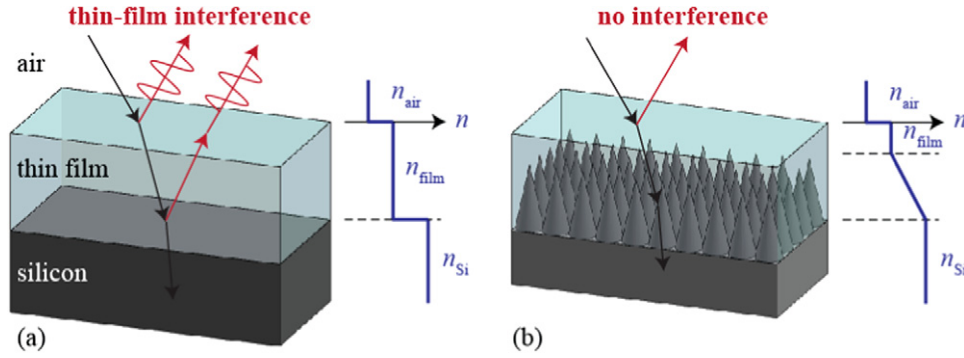


**Figure 1.** Schematic of (a) thin-film interference, where reflections from the film–silicon interface and top of the film interfere. (b) A nanostructured interface can be integrated between the film–silicon stack to suppress the interfacial reflection and eliminate thin-film interference effects. The gradient-index profile is qualitatively illustrated.

for many optical applications, such as filters, Bragg reflectors and light trappers [24–28], in many cases they can be undesirable. When thin films are used for electrical and mechanical purposes, namely as electrodes and protective layers, they inevitably lead to losses in optical transmission. Strong interfacial reflections can also reduce external quantum efficiencies in solar devices, in which case the reflected light does not enter the active material [27, 28]. Recent work by Jiang *et al* has demonstrated that the introduction of discrete porous multilayers between indium tin oxide (ITO) and silicon is effective in the suppression of such interfacial reflection and can improve solar cell efficiency [30].

In this work, we demonstrate an alternative approach using nanostructures to reduce such interfacial reflections and suppress thin-film interference effects. In this approach, a composite structure consisting of subwavelength nanocone arrays constructed from the bottom material is infiltrated by the material above, as illustrated in figure 1(b). This creates a gradient-index medium where the effective index varies gradually from those of the bottom to the top materials, eliminating the index mismatch. By reducing the interfacial reflection, only the reflection from the polymer top surface remains and thin-film interference effects can be eliminated. The interfacial nanostructures also ensure that any light that entered the film will transmit into the substrate with high efficiency. The proposed design is based on the moth-eye principle, but implemented at a material interface instead of the surface. While figure 1 illustrates the effect of a single thin film on a substrate, this principle of interfacial AR nanostructures can be extended to multiple interfaces of different materials, enabling light to transmit through multilayer devices without any reflection losses.

## 2. Simulation of the AR effect at a material interface

The AR effect at the nanostructured interface between a thin film and a substrate can be studied using a thin-film interference model. In this model, the reflections from the film surface and film–silicon interface interfere to create intensity oscillation, resulting in the colored appearance of thin films (figure 1). Using wave optics, the electric field of

light reflection from the top of the film and the film–silicon interface are given by

$$E_1 = A_1 \exp[-j(k \sin \theta_1 x + k \cos \theta_1 y)] \quad (1)$$

$$E_2 = A_2 \exp[-j(k \sin \theta_1 x + k \cos \theta_1 y + \psi)] \quad (2)$$

where  $k = 2\pi/\lambda$  is the wavevector and  $A_1$  and  $A_2$  are the respective field amplitudes. The optical path difference (OPD) between the two beams results in a phase difference  $\psi = 2nkd \cos \theta_2$ , where  $n$  and  $d$  are the film index and thickness, respectively, and  $\theta_2$  is the refracted angle inside the film. The intensities of the reflected beams are then  $R_1 = A_1^2$  and  $R_2 = A_2^2$ , where  $R_1$  is described by the Fresnel equation and  $R_2$  is determined by the effectiveness of the interfacial nanostructure. Note that secondary reflection of  $R_2$  at the air–polymer interface is ignored. The interference pattern of the two co-propagating beams is

$$I = |E_1 + E_2|^2 = I_o \left[ 1 + m \cos \left( \frac{2\pi}{\lambda} 2nd \cos \theta_2 \right) \right] \quad (3)$$

where

$$I_o = R_1 + R_2 \quad (4)$$

$$m = \frac{2\sqrt{R_1 R_2}}{R_1 + R_2} \quad (5)$$

In these equations  $I_o$  is the average intensity in the reflection, while  $m$  dictates the fringe visibility of the interference effect. Equation (4) indicates that as the interfacial reflection ( $R_2$ ) is reduced, the total reflected intensity will approach  $R_1$ , which is due to reflection on the air–polymer interface. In addition, equation (5) shows that  $m$  will approach zero as  $R_2$  is reduced, indicating the suppression of interference effects. It is important to note that the average reflection and contrast do not depend on film thickness, since the proposed AR effect is not based on interference.

## 3. Fabrication methods and materials

We demonstrate the integration of interfacial AR nanostructures at the interface between a thin polymer film and silicon substrates. The nanostructured interface is fabricated by first

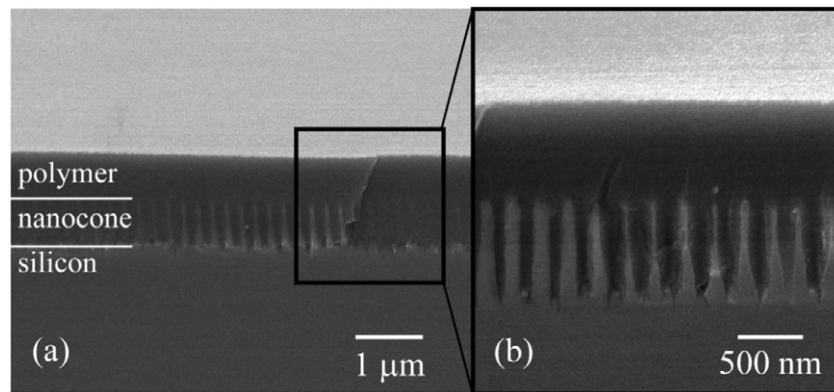


**Figure 2.** Micrographs of the fabricated nanostructured medium at the interface between a polymer film and silicon substrate (sample Si01): (a) cross-section view and (b) higher magnification images of the periodic nanocone structure infiltrated with polymer to create the interfacial nanostructures.

etching a nanocone array into silicon surface, followed by a subsequent polymer infiltration step (see supplementary information A, available at [stacks.iop.org/Nano/24/235202/mmedia](http://stacks.iop.org/Nano/24/235202/mmedia), for more information). In this process, the silicon substrate is coated with 170 nm of hydrogen silsesquioxane (HSQ; Dow Corning FOX16), 70 nm of antireflection coating (ARC; Brewer Science i-con-11), and 200 nm of photoresist (Sumitomo PFI-88A2). Laser interference lithography (IL) is used to create a two-dimensional array photoresist pattern [10, 31]. The ARC coating is used to reduce reflection from the resist layer during lithography. The pattern is then transferred into the silicon substrate using  $O_2$ ,  $CHF_3$  and  $Cl_2$  reactive ion etching (RIE). Five silicon nanocone samples (Si01–Si05) of the same period (235 nm) were fabricated with different  $Cl_2$  RIE etching times to tailor the structure height and profile. Micrographs of the fabricated profiles for samples Si02–Si05 are shown in supplementary information B (available at [stacks.iop.org/Nano/24/235202/mmedia](http://stacks.iop.org/Nano/24/235202/mmedia)).

A polymer film (Sumitomo PFI-88A7) is then spin-coated on the nanocone samples, infiltrating the surface structure and creating the nanostructured silicon–polymer interface. Cross-section scanning electron micrograph (SEM) images for sample Si01 are shown in figure 2. The nanocone array has period of 235 nm, height of 630 nm and base diameter of 180 nm, and the overlaying polymer has a thickness of 730 nm. Higher magnification micrograph indicates that there are no voids in the nanostructured medium, as shown in figure 2(b), indicating that the polymer was able to fully infiltrate the surface topography during the coating process. A polymer film on silicon sample with planar interface was prepared for comparison, also with a thickness of 730 nm.

#### 4. Results and discussion

The broadband reflectance of the fabricated polymer on silicon samples with planar and nanostructured interfaces (sample Si01) are measured, as plotted in figure 3. The light source used was non-polarized Xe light at incident angle of  $7.5^\circ$ . The solid lines represent the measured data and

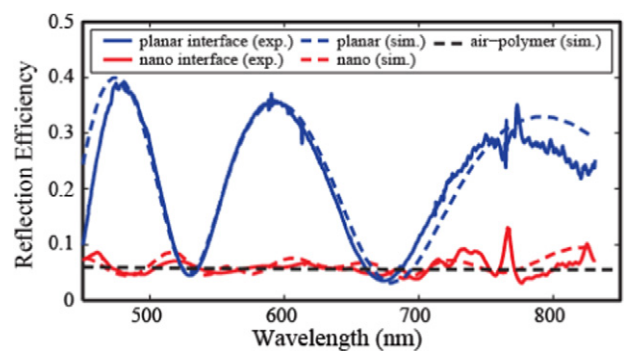


**Figure 3.** Measured broadband reflectance of the polymer–silicon sample with planar and nanostructured (sample Si01) interfaces. The thin-film interference effect is suppressed in the nanostructured sample. Both samples have 730 nm thick polymer layers and were measured at an incident angle of  $7.5^\circ$ . The reflection of the top air–polymer interface calculated using the Fresnel equation is also plotted for comparison.

the dashed lines are the corresponding theoretical simulation using rigorous coupled wave analysis (RCWA) [32, 33]. Details of the RCWA modeling are outlined in supplementary information C (available at [stacks.iop.org/Nano/24/235202/mmedia](http://stacks.iop.org/Nano/24/235202/mmedia)). Strong intensity oscillation in the reflectance profile can be observed for the sample with planar interface, characteristic of thin-film interference. The oscillation contrast,  $m = (I_{\max} - I_{\min}) / (I_{\max} + I_{\min})$ , measures the degree of fringe visibility and is calculated to be 0.8 for the planar interface sample. In comparison, the oscillation effect is significantly reduced for the sample with a nanostructured interface, and the measured reflection spectrum has a uniform response. The fringe contrast is calculated to be 0.15, a reduction of more than five-fold. This demonstrates the ability of the interfacial nanostructures to suppress the reflection at the material interface, which in turn suppresses the thin-film interference effect. The interfacial nanostructures also suppress the total reflection energy, reducing the average reflected efficiency from 23 to 6%. The remaining reflection can be attributed to reflection at the polymer (index of 1.65) top surface, which is not AR-treated in this work.

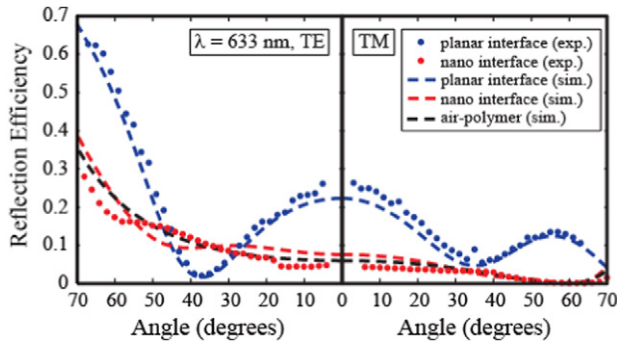


**Figure 4.** Measured angle-dependent reflection efficiencies of the polymer-silicon samples with planar and nanostructured (sample Si01) interfaces for TE and TM polarization.

For comparison, the reflectance for only the air-polymer interface (both semi-infinite media) is calculated using Fresnel equations, shown as the dashed line in figure 3. By eliminating the reflection from the polymer-silicon interface, the reflectance of the nanostructured sample resembles a simple polymer substrate having a single air-polymer interface. Note that the goal of the present study is to eliminate the interfacial reflection and thin-film interference effects. The top polymer surface can also be textured with AR nanostructures if overall reflection is to be reduced.

The angular-dependent reflection efficiency of the fabricated samples is characterized using a HeNe laser ( $\lambda = 633$  nm) for both TE and TM polarization, as shown in figure 4. The solid and dashed lines represent experimental data and the corresponding RCWA simulation, respectively. The reflection of TE-polarized light for the planar interface sample exhibits angle-dependent oscillation that is characteristic of thin-film interference, reaching a minimum at  $37^\circ$ . In comparison, the reflection profile of the nanostructured interface sample is more gradual and has suppressed intensity oscillation. The TM-polarization measurements exhibit similar trends. Note that the reflection for the nanostructured interface sample reaches nearly zero at around  $58^\circ$ , which corresponds to the Brewster angle for the top air-polymer interface. At this angle, the reflections at both air-polymer and polymer-silicon interfaces are zero, resulting in all light being transmitted. Similar to the broadband measurements, the nanostructured interface sample exhibits reflection behavior that is nearly identical to that of a polymer substrate, which is plotted as the black dashed lines. In this manner the underlying silicon does not contribute to any reflection, and any light in the polymer film can transmit through the polymer-silicon interface with no losses.

The effect of the interfacial reflection  $R_2$  on total reflection and thin-film interference effects can be compared to the model derived in equations (4) and (5). Since  $R_2$  cannot be directly measured, it is approximated by first measuring the surface reflection for the nanocone samples prior to coating polymer ( $R'_2$ ) and then scaling by a correction factor. This factor is derived from the Fresnel equation with zero incident angle:

**Table 1.** Experimentally measured average intensity and contrast of interference effects in the reflectance measurements for the fabricated samples.

Samples	Measured $R'_2$	Calculated $R_2$	Measured $I_o$	Measured $m$
Planar	0.33	0.15	0.20	0.80
Si01	0.0012	0.0006	0.058	0.15
Si02	0.0022	0.001	0.069	0.39
Si03	0.0045	0.002	0.068	0.47
Si04	0.011	0.005	0.072	0.58
Si05	0.023	0.011	0.081	0.86

$$R_2 = \frac{R_{\text{film-Si}}}{R_{\text{air-Si}}} R'_2 \quad (6)$$

where  $R_{\text{film-Si}} = (n_{\text{film}} - n_{\text{Si}})^2 / (n_{\text{film}} + n_{\text{Si}})^2$  and  $R_{\text{air-Si}} = (n_{\text{air}} - n_{\text{Si}})^2 / (n_{\text{air}} + n_{\text{Si}})^2$  are reflection coefficients at the polymer-silicon and air-silicon interfaces, respectively. This approximates the reflection at the silicon interface when the ambient medium is changed from air to polymer. Note that equation (6) is only valid near normal incidence, and polarization effects will have to be taken into account at oblique incidence angles. The  $I_o$  and  $m$  of samples Si01-Si05 are calculated from  $I_{\text{max}}$  and  $I_{\text{min}}$  identified on their respective broadband reflectance measurements (the raw broadband data are shown in supplementary information D (available at [stacks.iop.org/Nano/24/235202/mmedia](http://stacks.iop.org/Nano/24/235202/mmedia))). The incident angle is  $7.5^\circ$  for the measurements to ensure that equation (6) is valid. The results are tabulated in table 1, along with the measured  $R'_2$  and calculated  $R_2$  for the five nanostructured and one planar interface samples. The effect of interfacial reflection  $R_2$  on the average reflection efficiency and fringe contrast can be observed.

The experimentally measured average reflection intensity  $I_o$  and fringe contrast  $m$  from table 1 are plotted as functions of the interfacial reflection  $R_2$ , along with the model described in equations (4) and (5), as shown in figure 5. The sample types are denoted in figure 5(a), and they correspond to the data points with the same  $R_2$  in figure 5(b). The nanostructured interface exhibits strong interfacial AR effects, suppressing both  $I_o$  and  $m$ . The  $I_o$  value for the stack with a planar interface is noted as the right-most data point, which is roughly the average of the reflections from the top and bottom of the polymer layer. By introducing the interfacial nanostructures, as shown in the leftmost five points for samples Si01-Si05,  $I_o$  decreases dramatically as the reflection from the polymer-silicon interface is reduced. In the event when the interfacial reflection is completely eliminated, the  $I_o$  will approach the reflection efficiency of the top polymer layer, which is around 6% for the polymer used, as predicted by equation (4). The fringe contrast  $m$  also scales favorably at low interfacial reflection, approaching zero to indicate the absence of thin-film interference effects. However, since  $m$  scales as the square root of  $R_2$ , as shown in equation (5), a significant AR effect at the material interface is required. Sample Si05 has a poor AR effect due to its sub-optimal structure profile, and the fringe contrast is 0.86. Note that this value is higher than the sample with a planar interface,

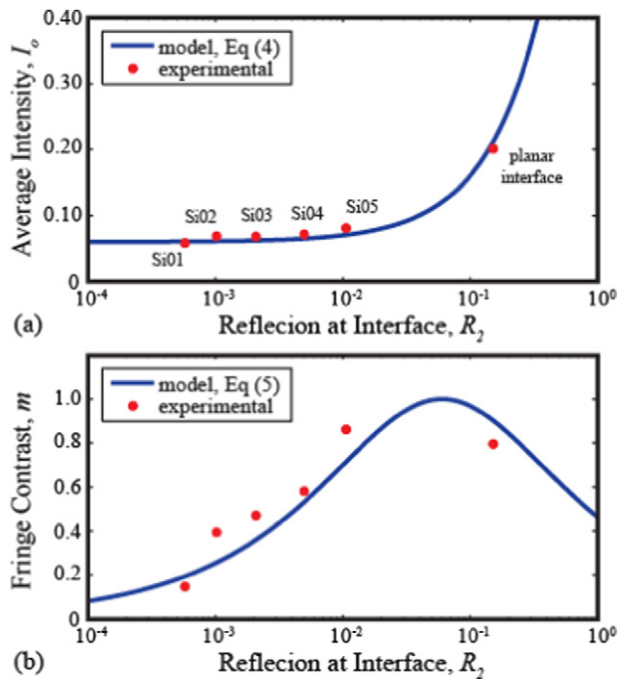


**Figure 5.** Measured (a) average reflection intensity  $I_o$  and (b) reflectance oscillation fringe contrast  $m$  for polymer–silicon samples with nanostructured and planar interfaces as functions of interfacial reflection  $R_2$ . The nanostructured samples were processed with different etch recipes to vary the taper profile and the degree of AR effect.

even though  $I_o$  has been decreased. Since contrast measures the amplitude balance of the interference waves, it reaches the maximum value of unity when reflections from the film surface and polymer–silicon interface are equal. These results and the derived model indicate that by using interfacial nanostructures, the reflection between two materials can be heavily suppressed. This effect in turn suppresses thin-film interference, allowing for wavelength/angle-independent optical behavior. For better interfacial AR effects than those demonstrated, taller structures [10] with an optimal taper profile can be used [34, 35].

The AR effects of the nanostructured interface can be visually observed at different viewing angles, as shown in figure 6. The polymer-coated samples with nanostructured (sample Si01) and planar interface were placed under white light next to a bare silicon substrate. The silicon sample has high broadband reflectance, resembling a colorless mirror at both viewing angles. For the polymer sample with a planar interface, the reflectance is wavelength sensitive and the sample appears colored. Changing the viewing angle also changes the color, characteristic of angle dependency in thin-film interference. In comparison, the polymer sample with a nanostructured interface appears dark and colorless, since the reflection at the material interface has been suppressed to eliminate thin-film interference effects. The sample is also colorless at both viewing angles, confirming the broadband and wide-angle AR response. Note the polymer thickness varies at the sample corners due to spin-coating edge effects, which leads to different colors for the sample with

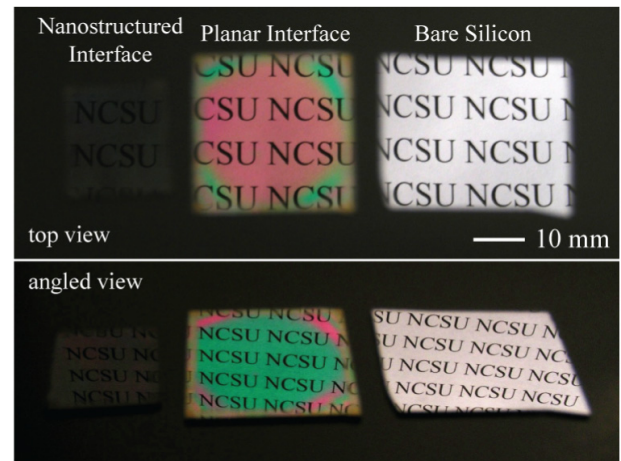


**Figure 6.** Top and angled views of the polymer–silicon samples with nanostructured (sample Si01) and planar interfaces next to a bare silicon substrate. Under white light illumination, the colored appearance induced by thin-film interference can be observed for the sample with a planar interface but not the sample with a nanostructured interface.

a planar interface but not the sample with a nanostructured interface.

## 5. Conclusion

In this work we demonstrate AR effects at the interface between two materials using interfacial nanostructures and the suppression of interference effects in thin films. The nanostructured interface creates an optical impedance-matching medium, resulting in a continuously varying refractive-index profile between the two neighboring materials. This principle was demonstrated in silicon substrates coated with a polymer thin film, where the nanostructured interface is able to reduce the reflection at the polymer–silicon interface. The samples were patterned in silicon using interference lithography, and the polymer film was spin-coated to create the nanostructured interface. This effect can be accurately described by the developed contrast model, which predicts the average intensity and contrast of the reflectance oscillation based on the AR performance of the interfacial nanostructures. This principle can also be applied to other materials and multilayer architectures, and lead to optical and optoelectronic devices with reduced wavelength and angle sensitivity and increased optical transmission.

## Acknowledgments

We gratefully acknowledge the students, staff and facility support from the North Carolina State University Nanofabrication Facility (NNF). This work was supported by a NASA Office of the Chief Technologist's Space Technology Research Opportunity—Early Career Faculty grant (grant NNX12AQ46G) and by the National Science Foundation (grant EEC-1160483) through the Nanosystems Engineering Research Center for Advanced Self-Powered Systems of Integrated Sensors and Technologies (ASSIST).

## References

- [1] Clapham P B and Hutley M C 1973 Reduction of lens reflexion by the 'moth eye' principle *Nature* **244** 281–2
- [2] Vukusic P and Sambles J R 2003 Photonic structures in biology *Nature* **424** 852–5
- [3] Stavenga D G, Foletti S, Palasantzas G and Arikawa K 2006 Light on the moth-eye corneal nipple array of butterflies *Proc. Biol. Sci.* **273** 661–7
- [4] Parker A R et al 2007 Biomimetics of the photonic nanostructures *Nature Nanotechnol.* **2** 347–53
- [5] Wilson S J and Hutley M C 1982 The optical properties of 'moth eye' antireflection surfaces *Opt. Acta: Int. J. Opt.* **29** 993–1009
- [6] Kanamori Y, Sasaki M and Hance K 1999 Broadband antireflection gratings fabricated upon silicon substrates *Opt. Lett.* **24** 1422–4
- [7] Boden S A and Bagnall D M 2008 Tunable reflection minima of nanostructured antireflective surfaces *Appl. Phys. Lett.* **93** 133108
- [8] Lalanne P and Morris G M 1997 Antireflection behavior of silicon subwavelength periodic structures for visible light *Nanotechnology* **8** 53–6
- [9] Song Y M, Yu J S and Lee Y T 2010 Antireflective submicrometer gratings on thin-film silicon solar cells for light-absorption enhancement *Opt. Lett.* **35** 276–8
- [10] Park K-C, Choi H J, Chang C-H, Cohen R E, McKinley G H and Barbastathis G 2012 Nanotextured silica surfaces with robust superhydrophobicity and omnidirectional broadband supertransmissivity *ACS Nano* **5** 3789–99
- [11] Sun C-H, Jiang P and Jiang B 2008 Broadband moth-eye antireflection coatings on silicon *Appl. Phys. Lett.* **92** 061112
- [12] Min W-L, Jiang B and Jiang P 2008 Bioinspired self-cleaning antireflection coatings *Adv. Mater.* **20** 3914–8
- [13] Chen H L, Chuang S Y, Lin C H and Lin Y H 2007 Using colloidal lithography to fabricate and optimize sub-wavelength pyramidal and honeycomb structures in solar cells *Opt. Express* **15** 14793–803
- [14] Chang C-H, Dominguez-Caballero J A, Choi H J and Barbastathis G 2011 Nanostructured gradient-index antireflection diffractive optics *Opt. Lett.* **36** 2354
- [15] Huang Y-F et al 2007 Improved broadband and quasi-omnidirectional anti-reflection properties with biomimetic silicon nanostructures *Nature Nanotechnol.* **2** 770–4
- [16] Xie G, Zhang G, Lin F, Zhang J, Liu Z and Mu S 2008 The fabrication of subwavelength anti-reflective nanostructures using a bio-template *Nanotechnology* **19** 095605
- [17] Ko D-H, Tumbleston J R, Henderson K J, Euliss L E, DeSimone J M, Lopez R and Samulski E T 2011 Biomimetic microlens array with antireflective 'moth-eye' surface *Soft Matter* **7** 6404
- [18] Choi K, Park S H, Song Y M, Lee Y T, Hwangbo C K, Yang H and Lee H S 2010 Nano-tailoring the surface structure for the monolithic high-performance antireflection polymer film *Adv. Mater.* **22** 3713–8
- [19] Paivanranta B, Saastamoinen T and Kuittinen M 2009 A wide-angle antireflection surface for the visible spectrum *Nanotechnology* **20** 375301
- [20] Xi J-Q, Schubert M F, Kim J K, Schubert E F, Chen M, Lin S-Y, Liu W and Smart J A 2007 Optical thin-film materials with low refractive index for broadband elimination of Fresnel reflection *Nature Photon.* **1** 176–9
- [21] Kuo M-L, Poxson D J, Kim Y S, Mont F W, Kim J K, Schubert E F and Lin S-Y 2008 Realization of a near-perfect antireflection coating for silicon solar energy utilization *Opt. Lett.* **33** 2527–9
- [22] Jung J-Y, Guo Z, Jee S-W, Um H-D, Park K-T and Lee J-H 2010 A strong antireflective solar cell prepared by tapering silicon nanowires *Opt. Express* **18** A286–92
- [23] Zhu J, Hsu C-M, Yu Z, Fan S and Cui Y 2010 Nanodome solar cells with efficient light management and self-cleaning *Nano Lett.* **10** 1979–84
- [24] Wang K X, Yu Z, Liu V, Cui Y and Fan S 2012 Absorption enhancement in ultrathin crystalline silicon solar cells with antireflection and light-trapping nanocone gratings *Nano Lett.* **12** 1616–9
- [25] Deceglie M G, Ferry V E, Alivisatos A P and Atwater H A 2012 Design of nanostructured solar cells using coupled optical and electrical modeling *Nano Lett.* **12** 2894–900
- [26] Ko D-H, Tumbleston J R, Gadisa A, Aryal M, Liu Y, Lopez R and Samulski E T 2011 Light-trapping nano-structures in organic photovoltaic cells *J. Mater. Chem.* **21** 16293–303
- [27] Betancur R, Martínez-Otero A, Elias X, Romero-Gómez P, Colodrero S, Miguez H and Martorell J 2012 Optical interference for the matching of the external and internal quantum efficiencies in organic photovoltaic cells *Sol. Energy Mater. Sol. Cells* **104** 87–91
- [28] Beiley Z M and McGehee M D 2012 Modeling low cost hybrid tandem photovoltaics with the potential for efficiencies exceeding 20% *Energy Environ. Sci.* **5** 9173–9
- [29] Pignalosa P, Liu B, Chen H, Smith H and Yi Y 2012 Giant light extraction enhancement of medical imaging scintillation materials using biologically inspired integrated nanostructures *Opt. Lett.* **37** 2808–10
- [30] Jang J, Song Y M, Yeo C I, Park C Y, Yu J S and Lee Y T 2011 Antireflective property of thin film a-Si solar cell structures with graded refractive index structure *Opt. Express* **19** A108–17
- [31] Smith H I 2001 Low cost nanolithography with nanoaccuracy *Physica E* **11** 104
- [32] Moharam M G, Grann E B and Pommet D A 1995 Formulation for stable and efficient implementation of the rigorous coupled-wave analysis of binary gratings. *J. Opt. Soc. Am. A* **12** 1068–76
- [33] Moharam M G, Pommet D A, Grann E B and Gaylord T K 1995 Stable implementation of the rigorous coupled-wave analysis for surface-relief gratings: enhanced transmittance matrix approach *J. Opt. Soc. Am. A* **12** 1077–86
- [34] Grann E B, Varga M G and Pommet D A 1995 Optimal design for antireflective tapered two-dimensional subwavelength grating structures *J. Opt. Soc. Am. A* **12** 333–9
- [35] Zhang Y, Li C and Loncar M 2013 Optimal broadband antireflective taper *Opt. Lett.* **38** 646–8